EUROPEAN JOURNAL OF COMPUTATIONAL MECHANICS, 2016
VOL. 25, NOS. 1–2, 2–23
http://dx.doi.org/10.1080/17797179.2016.1181029

Taylor & Francis
Taylor & Francis Group

Natural convection flow of a nanofluid in an enclosure under an inclined uniform magnetic field

Münevver Tezer-Sezgin[a], Canan Bozkaya[a], Önder Türk[b]

[a]Department of Mathematics, Middle East Technical University, Ankara, Turkey; [b]Department of Mathematics, Gebze Technical University, Kocaeli, Turkey

ABSTRACT

In this study, the natural convection in a square enclosure filled with water-based aluminium oxide (Al_2O_3) under the influence of an externally applied inclined magnetic field is considered numerically. The flow is steady, two-dimensional and laminar; the nanoparticles and water are assumed to be in thermal equilibrium. The governing equations are solved in terms of stream function–vorticity–temperature using both the dual reciprocity boundary element method and the finite element method to see the influence of characteristic flow parameters, namely: solid volume fraction (ϕ), inclination angle (γ), Rayleigh (*Ra*) and Hartmann (*Ha*) numbers. Numerical simulations are performed for $0 \leq \phi \leq 0.2$, $\gamma = 0, \pi/4, \pi/3, \pi/2$, and the values of Rayleigh and Hartmann numbers up to 10^7 and 300, respectively. The results show that the buoyancy-driven circulating flows undergo inversion of direction as *Ra* and *Ha* increase, and magnitudes of streamlines and vorticity contours increase as *Ra* increases, but decrease as *Ha* increases. The isotherms have a horizontal profile for high *Ra* values as a result of convective dominance over conduction. As *Ha* increases, effect of the convection on flow is reduced, thus the isotherms tend to have vertical profiles.

ARTICLE HISTORY
Received 22 October 2015
Accepted 21 February 2016

KEYWORDS
DRBEM; FEM; natural convection; nanofluid; magnetic field

1. Introduction

The problems of natural convection under the influence of a magnetic field have received considerable attention over the last decades due to their wide variety of engineering applications, such as crystal growth, purification of molten metals, nuclear reactor cooling, microelectronic devices and solar technology. The nanofluid is a liquid–solid mixture in which metallic or non-metallic nanoparticles are suspended. The suspended particles change the transport properties and heat transfer performance of the fluid, which exhibits a great potential in enhancing heat transfer. Thus, the mechanism of heat transfer of nanofluids has been recently investigated by many researchers using different numerical

CONTACT Münevver Tezer-Sezgin munt@metu.edu.tr

methods in different geometries. When the fluid is also electrically conducting, an external magnetic field can be used to control the convection within enclosures.

Öztop, Al-Salem, and Pop (2011) studied the mixed convection with a magnetic field in a top-sided lid-driven cavity heated by a corner heater. Yu, Qiu, Qiu, and Tian (2013) numerically investigated the natural convection in a rectangular cavity under different directions of uniform magnetic field. Both of these studies showed that heat transfer decreases with an increase in the intensity of external magnetic field (as Hartmann number increases). Sheikholeslami and Ganji (2014) used control volume-based finite element method (FEM) to study the effect of external magnetic field on ferrofluid flow and heat transfer in a semi-annulus enclosure with sinusoidal hot wall. Pirmohammadi and Ghassemi (2009) studied the effect of magnetic field on convection heat transfer inside a tilted square enclosure. In trapezoidal cavities, MHD natural and free convections are studied by Hasanuzzaman et al. (2012) and Hossain and Alim (2014), respectively. Türk and Tezer-Sezgin (2013) have given FEM solution of natural convection flow in square enclosures under magnetic field. As discussed in the above studies, magnetic field results in the decrease of convective circulating flows within the enclosures filled with electrically conducting fluids, consequently reducing the rate of heat transfer. But, in some devices, such as magnetic field sensors and cooling system of electronic devices, enhanced heat transfer is desired. In order to improve the heat transfer performance of such devices, the use of nanofluids with higher thermal conductivity is a promising solution.

The natural convection in a square enclosure filled with a nanofluid under the effect of a magnetic field is investigated numerically in many works. The effects of parameters such as the Rayleigh number, the Hartmann number and the nanofluid solid volume fraction on the flow and temperature fields are analysed using different numerical techniques in these studies. A finite element approach using COMSOL Multiphysics is implemented in Hamida and Charrada (2015), whereas the control volume formulation SIMPLE algorithm and a finite volume code based on PATANKAR's SIMPLER method are used in the works of Ghasemi, Aminossadati, and Raisi (2011) and Pirmohammadi and Ghassemi (2009), respectively. On the other hand, the natural convection in a triangular enclosure filled with nanofluid in presence of horizontally applied magnetic field and partially heated by differently located heat sources is solved by finite volume method in Mahmoudi, Pop, and Shahi (2012), and the numerical results are obtained up to the values of $Ra = 10^7$ and $Ha = 100$. A control volume formulation using the SIMPLE algorithm was developed in Ghasemi (2013) to study the natural convection in a U-shaped enclosure which is filled with a nanofluid. It is observed that the heat transfer rate increases with an increase in Rayleigh number and the solid volume fraction, but it decreases with an increase in the Hartmann number. Further, the MHD natural convection in a nanofluid-filled inclined enclosure with sinusoidal wall is investigated using the control volume-based FEM in the work of Sheikholeslami, Gorji-Bandpy, Ganji, and

Soleimani (2014). The problem of natural convection under the influence of an inclined magnetic field in an inclined L-shaped enclosure with differentially heated wall, and filled with water–Cu nanofluid is analysed in Elshehabey, Hady, Ahmed, and Mohamed (2014). The fully implicit finite difference method is used to solve the governing equations for $Ra = 10^6$ and $Ha = 100$ and different angles of inclination and magnetic field directions. Lattice Boltzmann method has also been used in solving MHD natural convection of water/alumina nanofluids by Kefayati (2013) and Sheikholeslami, Gorji-Bandpy, and Ganji (2013). It is found that the enhancement in heat transfer is an increasing function of Hartmann number, while it is a decreasing function of Rayleigh number in Sheikholeslami, Gorji-Bandpy, and Ganji (2013). As a boundary discretization technique, the dual reciprocity boundary element method (DRBEM) solution of the unsteady natural convective flow of nanofluids in a square enclosure with a heat source is presented in Gümgüm and Tezer-Sezgin (2010) in the absence of external magnetic field.

In the present study, the natural convection heat transfer in a square enclosure filled with a nanofluid in the presence of a magnetic field is considered. The main objective of this study is to solve the problem with two effective and accurate numerical methods, namely: FEM and DRBEM, and to compare these techniques which differ in nature as being domain and boundary discretization types, respectively. The DRBEM is a boundary-only discretization technique which enables one to use the fundamental solution of the Laplace equation due to the treatment of non-linear terms as inhomogeneity. Thus, the discretization of only the boundary of the region results in small algebraic systems, which constitutes the main advantage of DRBEM. On the other hand, the FEM, a well-developed and widely used reliable numerical approach, is capable of giving more accurate results, especially for very high characteristic flow parameters; however, it results in large-sized algebraic systems requiring high computational cost. In this paper, numerical tests are performed for a wide range of problem parameters such as Rayleigh number, Hartmann number and solid volume fraction. The external magnetic field is oblique and the solutions are obtained for large values of Hartmann number. The results are visualised in terms of streamlines, isotherms and vorticity contours to see the effect of buoyancy force, nanoparticles and magnetic field on the fluid flow and heat transfer.

2. Governing equations

The problem of a steady, two-dimensional, laminar natural convection flow of a Newtonian and incompressible nanofluid (water–Al_2O_3) is considered in a square enclosure under the effect of an externally applied magnetic field. The base fluid and the solid spherical nanoparticles are considered to be in thermal equilibrium, and their properties are taken from Ghasemi et al. (2011). The induced magnetic field, radiation and the Joule heating effects are neglected. The

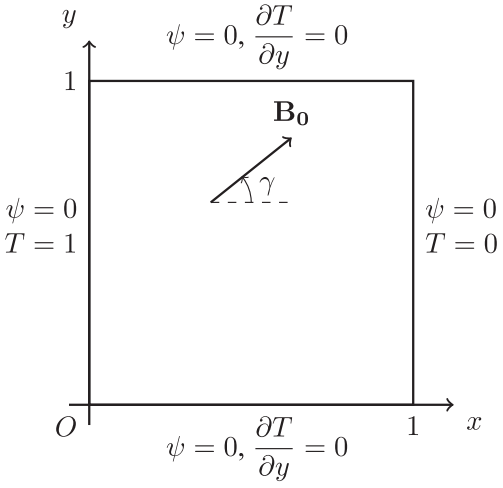

Figure 1. Domain and boundary conditions of the problem.

gravity is in the vertical direction and there is no viscous dissipation. No-slip boundary conditions for the velocity are imposed on the walls of the cavity. The upper and lower walls of the cavity are taken as adiabatic, whereas the vertical walls are kept at constant temperatures, namely: the left wall is heated (T_h) and the right wall is cooled (T_c). The variation of the density in the buoyancy term is determined by means of Boussinesq approximation and the other thermo-physical properties of the nanofluid are assumed as constant. The external magnetic field with intensity B_0 is uniform and is applied in a direction lying in the xy-plane but forming an angle γ with the x-axis (see Figure 1).

Under the above assumptions, the continuity, momentum and energy equations can be written in the non-dimensional velocity-pressure–temperature form as (Ghasemi et al., 2011; Ghasemi, 2013; Elshehabey et al., 2014)

$$\frac{\partial u}{\partial x} + \frac{\partial v}{\partial y} = 0 \tag{1}$$

$$u\frac{\partial u}{\partial x} + v\frac{\partial u}{\partial y} = -\frac{\partial p}{\partial x} + \frac{\mu_{nf}}{\rho_{nf}\alpha_f}\left(\frac{\partial^2 u}{\partial x^2} + \frac{\partial^2 u}{\partial y^2}\right) + Ha^2 Pr \sin\gamma \left(v\cos\gamma - u\sin\gamma\right) \tag{2}$$

$$u\frac{\partial v}{\partial x} + v\frac{\partial v}{\partial y} = -\frac{\partial p}{\partial y} + \frac{\mu_{nf}}{\rho_{nf}\alpha_f}\left(\frac{\partial^2 v}{\partial x^2} + \frac{\partial^2 v}{\partial y^2}\right) + RaPr\frac{(\rho\beta)_{nf}}{\rho_{nf}\beta_f}T + Ha^2 Pr \cos\gamma \left(u\sin\gamma - v\cos\gamma\right) \tag{3}$$

$$u\frac{\partial T}{\partial x} + v\frac{\partial T}{\partial y} = \frac{\alpha_{nf}}{\alpha_f}\left(\frac{\partial^2 T}{\partial x^2} + \frac{\partial^2 T}{\partial y^2}\right) \tag{4}$$

with the non-dimensional parameters

$$x = \frac{\bar{x}}{l},\ y = \frac{\bar{y}}{l},\ u = \frac{\bar{u}l}{\alpha_f},\ v = \frac{\bar{v}l}{\alpha_f},\ p = \frac{\bar{p}l^2}{\rho_{nf}\alpha_f^2},\ T = \frac{\overline{T} - T_c}{T_h - T_c},$$
$$Ra = \frac{g\beta_f \ell^3 (T_h - T_c)}{\nu_f \alpha_f},\quad Pr = \frac{\nu_f}{\alpha_f},\ Ha = B_0 \ell \sqrt{\frac{\sigma_{nf}}{\rho_{nf}\nu_f}} \tag{5}$$

where l, g, σ, ν and B_0 are the characteristic length, gravitational acceleration, electrical conductivity, kinematic viscosity and the magnetic field intensity, respectively. In Equations (1)–(4), the parameters u, v, p and T denote the non-dimensional x- and y-velocity components, pressure and temperature of the fluid, respectively. The overline in (5) indicates that the quantities are dimensional. Here, Ra is the Rayleigh number, Pr is the Prandtl number and Ha is the Hartmann number. The thermo-physical properties of water, aluminium oxide and the nanofluid are determined as (Ghasemi et al., 2011)

$$\rho_{nf} = (1-\phi)\rho_f + \phi\rho_p,\quad \sigma_{nf} = (1-\phi)\sigma_f + \phi\sigma_p,\quad \alpha_{nf} = k_{nf}/(\rho C_p)_{nf},$$
$$(\rho\beta)_{nf} = (1-\phi)(\rho\beta)_f + \phi(\rho\beta)_p,\quad (\rho C_p)_{nf} = (1-\phi)(\rho C_p)_f + \phi(\rho C_p)_p,$$
$$k_{nf} = k_f\left[\frac{k_p + 2k_f - 2\phi(k_f - k_p)}{k_p + 2k_f + \phi(k_f - k_p)}\right],\quad \mu_{nf} = \mu_f(1-\phi)^{-2.5} \tag{6}$$

where ϕ is the solid volume fraction, ρ is the density, α is the thermal diffusivity, C_p is the specific heat, β is the thermal expansion coefficient, μ is the effective dynamic viscosity, k is the thermal conductivity and the subscripts '$_{nf}$', '$_f$' and '$_p$' refer to nanofluid, fluid and nanoparticle, respectively.

For the two-dimensional flow, defining stream function $\psi(x,y)$ and vorticity $w(x,y)$ as

$$\frac{\partial\psi}{\partial y} = u,\quad \frac{\partial\psi}{\partial x} = -v,\quad w = \frac{\partial v}{\partial x} - \frac{\partial u}{\partial y}$$

the Equations (1)–(4) can be written in the stream function–vorticity and temperature

$$\nabla^2\psi = -w \tag{7}$$
$$\frac{\mu_{nf}}{\rho_{nf}\alpha_f}\nabla^2 w = \frac{\partial w}{\partial x}\frac{\partial\psi}{\partial y} - \frac{\partial w}{\partial y}\frac{\partial\psi}{\partial x} - RaPr\frac{(\rho\beta)_{nf}}{\rho_{nf}\beta_f}\frac{\partial T}{\partial x} - Ha^2 Pr\left(\sin(2\gamma)\frac{\partial^2\psi}{\partial x\partial y} + \cos^2\gamma\frac{\partial^2\psi}{\partial x^2} + \sin^2\gamma\frac{\partial^2\psi}{\partial y^2}\right) \tag{8}$$
$$\frac{\alpha_{nf}}{\alpha_f}\nabla^2 T = \frac{\partial T}{\partial x}\frac{\partial\psi}{\partial y} - \frac{\partial T}{\partial y}\frac{\partial\psi}{\partial x}. \tag{9}$$

Equations (7)–(9) are accompanied with the accordingly transformed boundary conditions as shown in Figure 1.

3. Numerical methods

3.1. DRBEM formulation

The aim of the DRBEM is to transform the governing equations of the problem into boundary integral equations by treating all the terms except Laplacian operator as inhomogeneity (Brebbia, Partridge, & Wrobel, 1992). In this manner, the governing Equations (7)–(9) are weighted with the two-dimensional fundamental solution of Laplace equation, $u^* = 1/2\pi \ln(1/r)$. The application of the Green's second identity to Equations (7)–(9) results in

$$c_i\psi_i + \int_\Gamma \left(q^*\psi - u^*\frac{\partial\psi}{\partial n}\right)\mathrm{d}\Gamma = -\int_\Omega (-w)u^*\mathrm{d}\Omega \tag{10}$$

$$\begin{aligned} c_i w_i + \int_\Gamma \left(q^* w - u^*\frac{\partial w}{\partial n}\right)\mathrm{d}\Gamma = -\int_\Omega \frac{\rho_{nf}\alpha_f}{\mu_{nf}}\Bigg[&\frac{\partial w}{\partial x}\frac{\partial\psi}{\partial y} - \frac{\partial w}{\partial y}\frac{\partial\psi}{\partial x} \\ &- RaPr\frac{(\rho\beta)_{nf}}{\rho_{nf}\beta_f}\frac{\partial T}{\partial x} \\ &- Ha^2 Pr\left(\sin(2\gamma)\frac{\partial^2\psi}{\partial x\partial y} + \cos^2\gamma\frac{\partial^2\psi}{\partial x^2}\right. \\ &\left.+ \sin^2\gamma\frac{\partial^2\psi}{\partial y^2}\right)\Bigg]u^*\mathrm{d}\Omega \end{aligned} \tag{11}$$

$$c_i T_i + \int_\Gamma (q^* T - u^*\frac{\partial T}{\partial n})\mathrm{d}\Gamma = -\int_\Omega \frac{\alpha_f}{\alpha_{nf}}(\frac{\partial T}{\partial x}\frac{\partial\psi}{\partial y} - \frac{\partial T}{\partial y}\frac{\partial\psi}{\partial x})u^*\mathrm{d}\Omega \tag{12}$$

where $q^* = \partial u^*/\partial n$, Γ is the boundary of the domain Ω and the subscript i denotes the source point. The constant c_i is given by $c_i = \theta_i/2\pi$ with the internal angle θ_i at the source point.

The integrands of the domain integrals on the right-hand side of Equations (10)–(12) except u^* are treated as inhomogeneity. Thus, they are approximated by a set of radial basis functions $f_j(x, y)$ linked with the particular solutions $\hat{u}_j$ to the equation $\nabla^2\hat{u}_j = f_j$ (Brebbia et al., 1992). The approximations for these integrands are given by $\sum_{j=1}^{N+L}\alpha_j f_j(x, y)$, $\sum_{j=1}^{N+L}\beta_j f_j(x, y)$ and $\sum_{j=1}^{N+L}\gamma_j f_j(x, y)$, respectively, for Equations (10)–(12). The coefficients α_j, β_j and γ_j are undetermined constants. The numbers of the boundary and the internal nodes are denoted by N and L, respectively. Now, the right-hand sides of Equations (10)–(12) also involve the multiplication of the Laplace operator with the fundamental solution u^*, which can be treated in a similar manner by the use of DRBEM to obtain the boundary-only integrals. Then, the use of constant elements for the discretization of the boundary results in the corresponding matrix–vector form

of Equations (10)–(12)

$$H\psi - G\frac{\partial \psi}{\partial n} = (H\hat{U} - G\hat{Q})F^{-1}\{-w\}, \tag{13}$$

$$\left(Hw - G\frac{\partial w}{\partial n}\right) = (H\hat{U} - G\hat{Q})F^{-1}\left\{\frac{\rho_{nf}\alpha_f}{\mu_{nf}}\left[\frac{\partial w}{\partial x}\frac{\partial \psi}{\partial y} - \frac{\partial w}{\partial y}\frac{\partial \psi}{\partial x} - RaPr\frac{(\rho\beta)_{nf}}{\rho_{nf}\beta_f}\frac{\partial T}{\partial x} - Ha^2Pr\left(\sin(2\gamma)\frac{\partial^2\psi}{\partial x\partial y} + \cos^2\gamma\frac{\partial^2\psi}{\partial x^2} + \sin^2\gamma\frac{\partial^2\psi}{\partial y^2}\right)\right]\right\} \tag{14}$$

$$\left(HT - G\frac{\partial T}{\partial n}\right) = (H\hat{U} - G\hat{Q})F^{-1}\left\{\frac{\alpha_f}{\alpha_{nf}}\left(\frac{\partial T}{\partial x}\frac{\partial \psi}{\partial y} - \frac{\partial T}{\partial y}\frac{\partial \psi}{\partial x}\right)\right\} \tag{15}$$

where the matrices $\hat{U}$ and $\hat{Q}$ are constructed by taking each of the vectors $\hat{u}_j$ and $\hat{q}_j$ as columns, respectively. The coordinate matrix F of size $(N + L)$ contains the radial basis functions f_j as columns (e.g. $f = 1 + r_j$). The components of the matrices H and G are

$$H_{ij} = c_i\delta_{ij} + \frac{1}{2\pi}\int_{\Gamma_j}\frac{\partial}{\partial n}\left(\ln\left(\frac{1}{r}\right)\right)\mathrm{d}\Gamma_j, \qquad H_{ii} = -\sum_{j=1, j\neq i}^{N} H_{ij},$$

$$G_{ij} = \frac{1}{2\pi}\int_{\Gamma_j}\ln\left(\frac{1}{r}\right)\mathrm{d}\Gamma_j, \qquad G_{ii} = \frac{A}{2\pi}\left(\ln\left(\frac{2}{A}\right) + 1\right)$$

where r is the distance from node i to element j, A is the length of the element and δ_{ij} is the Kronecker delta function. The resulting non-linear and coupled DRBEM equations are solved by an iterative process with initial estimates of vorticity and temperature. First, the stream function Equation (13) is solved by giving an initial estimate for vorticity. Then, with the use of an initial estimate for the temperature, the vorticity Equation (14) is solved. Once the vorticity values are obtained at all points in the domain, a similar procedure is employed for the solution of the energy Equation (15). In each iteration, the required space derivatives of the unknowns ψ, w and T, and also the unknown vorticity boundary conditions are obtained using the coordinate matrix F as

$$\frac{\partial R}{\partial x} = \frac{\partial F}{\partial x}F^{-1}R, \quad \frac{\partial R}{\partial y} = \frac{\partial F}{\partial y}F^{-1}R, \quad w = -\left(\frac{\partial^2 F}{\partial x^2}F^{-1}\psi + \frac{\partial^2 F}{\partial y^2}F^{-1}\psi\right)$$

where R is one of the unknowns ψ, w or T. The iterative procedure will stop when a pre-assigned tolerance is reached between two successive iterations.

3.2. FEM formulation

The FEM formulation of Equations (7)–(9) is obtained by extending the FEM model in Türk and Tezer-Sezgin (2013) for the natural convection of pure fluids

under the effect of an inclined magnetic field. The weak form is developed by multiplying Equations (7)–(9) with the weight functions ω_1, ω_2 and ω_3 which are assumed to be twice differentiable with respect to x and y, and taken as equal to the shape functions used for an element approximation in Galerkin approach (Reddy, 2006). Then, the application of the divergence theorem results in:

$$-\int_\Omega \left(\frac{\partial \omega_1}{\partial x}\frac{\partial \psi}{\partial x}+\frac{\partial \omega_1}{\partial y}\frac{\partial \psi}{\partial y}\right)\mathrm{d}\Omega+\int_\Omega \omega_1 w\mathrm{d}\Omega+\int_{\partial\Omega}\omega_1\frac{\partial \psi}{\partial n}\mathrm{d}s=0, \tag{16}$$

$$\begin{aligned}&-\frac{\mu_{nf}}{\rho_{nf}\alpha_f}\int_\Omega\left(\frac{\partial \omega_2}{\partial x}\frac{\partial w}{\partial x}+\frac{\partial \omega_2}{\partial y}\frac{\partial w}{\partial y}\right)\mathrm{d}\Omega-\int_\Omega\omega_2\left(\frac{\partial \psi}{\partial x}\frac{\partial w}{\partial y}-\frac{\partial w}{\partial y}\frac{\partial \psi}{\partial x}\right)\mathrm{d}\Omega\\&+Ha^2Pr\int_\Omega\omega_2\left(\sin(2\gamma)\frac{\partial^2\psi}{\partial x\partial y}+\cos^2\gamma\frac{\partial^2\psi}{\partial x^2}+\sin^2\gamma\frac{\partial^2\psi}{\partial y^2}\right)\mathrm{d}\Omega\\&+RaPr\frac{(\rho\beta)_{nf}}{\rho_{nf}\beta_f}\int_\Omega\omega_2\frac{\partial T}{\partial x}\mathrm{d}\Omega+\frac{\mu_{nf}}{\rho_{nf}\alpha_f}\int_{\partial\Omega}\omega_2\frac{\partial w}{\partial n}\mathrm{d}s=0,\end{aligned} \tag{17}$$

$$\begin{aligned}&-\frac{\alpha_{nf}}{\alpha_f}\int_\Omega\left(\frac{\partial \omega_3}{\partial x}\frac{\partial T}{\partial x}+\frac{\partial \omega_3}{\partial y}\frac{\partial T}{\partial y}\right)\mathrm{d}\Omega-\int_\Omega w_3\left(\frac{\partial T}{\partial x}\frac{\partial \psi}{\partial y}-\frac{\partial T}{\partial y}\frac{\partial \psi}{\partial x}\right)\mathrm{d}\Omega\\&+\frac{\alpha_{nf}}{\alpha_f}\int_{\partial\Omega}\omega_3\frac{\partial T}{\partial n}\mathrm{d}s=0,\end{aligned} \tag{18}$$

dropping the boundary integrals due to the property of shape functions to be vanished for Dirichlet boundary conditions, and zero normal derivative conditions. The region is discretized using 6-nodal triangular elements, and quadratic shape functions are used in the approximation of ψ, w and T over each element. Assembly procedure for all elements results in matrix–vector system of equations

$$[K]\{\psi\}=[M]\{w\} \tag{19}$$

$$\frac{\mu_{nf}}{\rho_{nf}\alpha_f}[K]\{w\}+[A]\{w\}=RaPr\frac{(\rho\beta)_{nf}}{\rho_{nf}\beta_f}\{F_1\}+Ha^2Pr\{F_2\} \tag{20}$$

$$\frac{\alpha_{nf}}{\alpha_f}[K]\{T\}+[A]\{T\}=\{0\} \tag{21}$$

where the stiffness, mass and convective matrices are given as

$$[K]=\sum_{e=1}^{M_e}\int_{\Omega_e}\left(\frac{\partial N_i^e}{\partial x}\frac{\partial N_j^e}{\partial x}+\frac{\partial N_i^e}{\partial y}\frac{\partial N_j^e}{\partial y}\right)\mathrm{d}\Omega_e$$

$$[M]=\sum_{e=1}^{M_e}\int_{\Omega_e}N_i^eN_j^e\mathrm{d}\Omega_e$$

$$[A]=\sum_{e=1}^{M_e}\int_{\Omega_e}N_i^e\left[\left(\sum_{k=1}^{6}\frac{\partial N_k^e}{\partial y}\psi_k^e\right)\frac{\partial N_j^e}{\partial x}-\left(\sum_{k=1}^{6}\frac{\partial N_k^e}{\partial x}\psi_k^e\right)\frac{\partial N_j^e}{\partial y}\right]\mathrm{d}\Omega_e,$$

for $i, j = 1, \ldots, 6$. The right-hand-side vectors are given as

$$\{F_1\} = \sum_{e=1}^{M_e} \int_{\Omega_e} N_i^e \sum_{k=1}^{6} \left(\frac{\partial N_k^e}{\partial x} T_k^e \right) \mathrm{d}\Omega_e$$

$$\{F_2\} = \sum_{e=1}^{M_e} \int_{\Omega_e} N_i^e \left(\sin(2\gamma) \sum_{k=1}^{6} \frac{\partial^2 N_k^e}{\partial x \partial y} \psi_k^e + \cos^2\gamma \sum_{k=1}^{6} \frac{\partial^2 N_k^e}{\partial x^2} \psi_k^e + \sin^2\gamma \sum_{k=1}^{6} \frac{\partial^2 N_k^e}{\partial y^2} \psi_k^e \right) \mathrm{d}\Omega_e.$$

Here, $i = 1, \ldots, 6$ and $\sum_{e=1}^{M_e}$ represents the assembly procedure over the total number of elements, M_e. In the computations of the element matrices and vectors, the integrations are carried out using an isoparametric interpolation and Gaussian quadrature. Equations (19)–(21) are solved iteratively, and the missing vorticity boundary values are calculated using the formula

$$w_b = -(a_0\psi_b + a_1\psi_p + a_2\psi_q + a_3\psi_n). \tag{22}$$

In (22), the subscript b denotes the boundary node, ψ_p and ψ_q are the stream function values, respectively, ph and qh distance away nodes along the normal direction, h being the distance between two consecutive nodes, and ψ_n is the normal derivative. The constants a_i, $i = 0, 1, 2, 3$, are derived from the Taylor series expansion of the stream function by means of Equation (7) (see Türk and Tezer-Sezgin (2013) for more details). In calculations, the nodes at the upper and lower corners are included to the upper and lower walls, respectively. The right-hand side vectors $\{F_1\}$ and $\{F_2\}$ are computed from previously obtained ψ and T values in each iteration. The iterative procedure is carried out until a convergence tolerance is reached between two successive iterations for all unknowns.

4. Results and discussion

The steady natural convection flow in an enclosure filled with a water–(Al_2O_3) nanofluid under the influence of a magnetic field is analysed by two powerful numerical techniques, DRBEM and FEM. The obtained numerical results are presented including a comparison of the two methods. Numerical tests are carried out for several values of Ra, Ha, γ and ϕ. Grid dependency is tested and the results are shown in Figure 2. It is observed that in DRBEM $N = 200$ constant boundary elements and in FEM $M_e = 1152$ quadratic triangular elements are enough to satisfy the grid independence. Thus, these numbers of elements are used in obtaining the results presented in this section. The convergence tolerance for the iterative procedures for each method is set to be 10^{-5}.

The comparison of the DRBEM and FEM solutions to the system (7)–(9) under the effect of a horizontally applied magnetic field ($\gamma = 0$) is displayed in

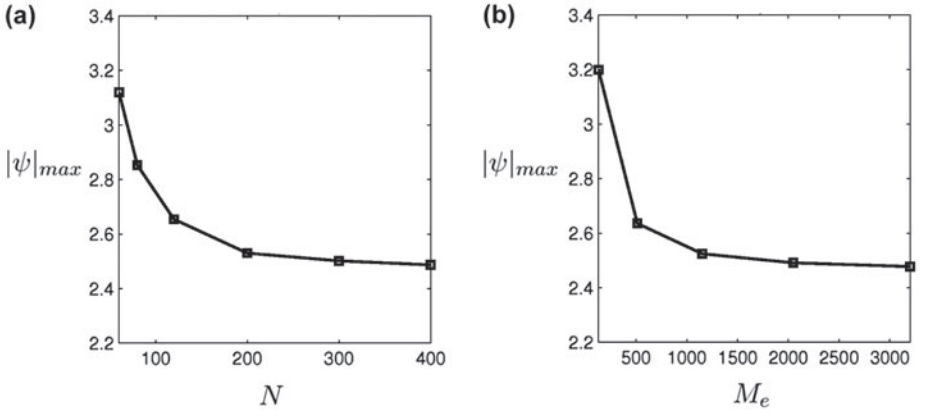

Figure 2. Grid dependency for $Ha = 60$, $Ra = 10^5$, $\phi = 0.03$ when $\gamma = 0$: (a) DRBEM, (b) FEM.

Figure 3 for the case when $Ha = 60$, $Ra = 10^5$, $\phi = 0.03$. These results show the agreement of the solutions obtained by both FEM and DRBEM methods which are also in well agreement with the solutions given in the work of Ghasemi et al. (2011). DRBEM and FEM have different characteristics as being boundary and domain discretization methods, respectively. DRBEM requires considerably less boundary elements compared to the number of domain elements (triangles) in FEM.

The effect of Rayleigh number on the streamlines, the equivorticity lines and the isotherms at $Ha = 60$, $\phi = 0.03$ in the case of horizontally applied magnetic field ($\gamma = 0$) by DRBEM is displayed in Figure 4. It is well observed that for small values of Rayleigh number ($Ra = 10^3, 10^4$), the streamlines show similar profiles; however, an increase in their magnitudes occurs as Ra increases. The core vortex of the streamlines tends to become diagonal at the highest Rayleigh number ($Ra = 10^5$, see Figure 3(a)). On the other hand, an increase in Ra to 10^5 leads the flow to become convection dominated. Thus, the isotherms change their profile from vertical to almost diagonal (see Figure 3(a)).

In Figure 5, the DRBEM solutions are shown at $Ra = 10^3$, $\phi = 0.03$, $\gamma = 0$ for three values of Hartmann number ($Ha = 100, 200, 300$). The values of both stream function and vorticity decrease gradually in magnitude with an increase in Hartmann number since the externally applied magnetic field has a retardation effect on the flow when its intensity gets stronger. Further, following the increase in Ha to 300, the core vortex in streamlines extends vertically and this results in the boundary layer formation along the horizontal walls of the cavity. This reduction in velocity causes a decrease in convective heat transfer. Thus, conduction heat transfer becomes the dominant mechanism in the heat transfer. The isotherms are almost vertical for all magnetic numbers due to the dominance in conduction for $Ra = 10^3$.

The variation in stream function, vorticity and temperature along the vertical centreline $x = 0.5$, $0 \leq y \leq 1$ at different solid volume fractions ($\phi =$

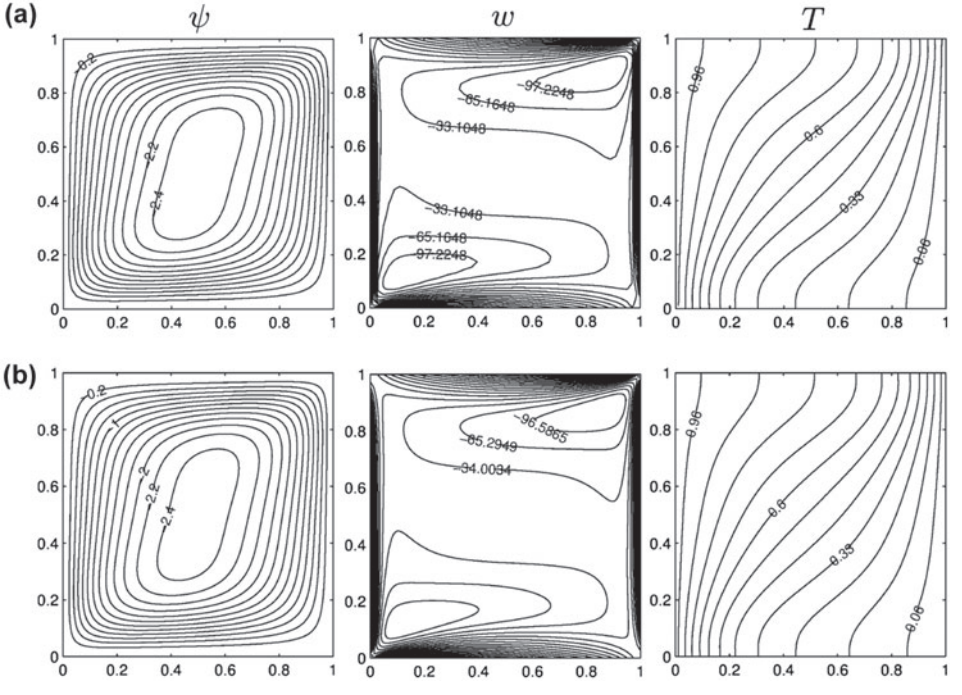

Figure 3. Streamlines, vorticity contours and isotherms for $Ha = 60$, $Ra = 10^5$, $\phi = 0.03$ when $\gamma = 0$: (a) DRBEM, (b) FEM.

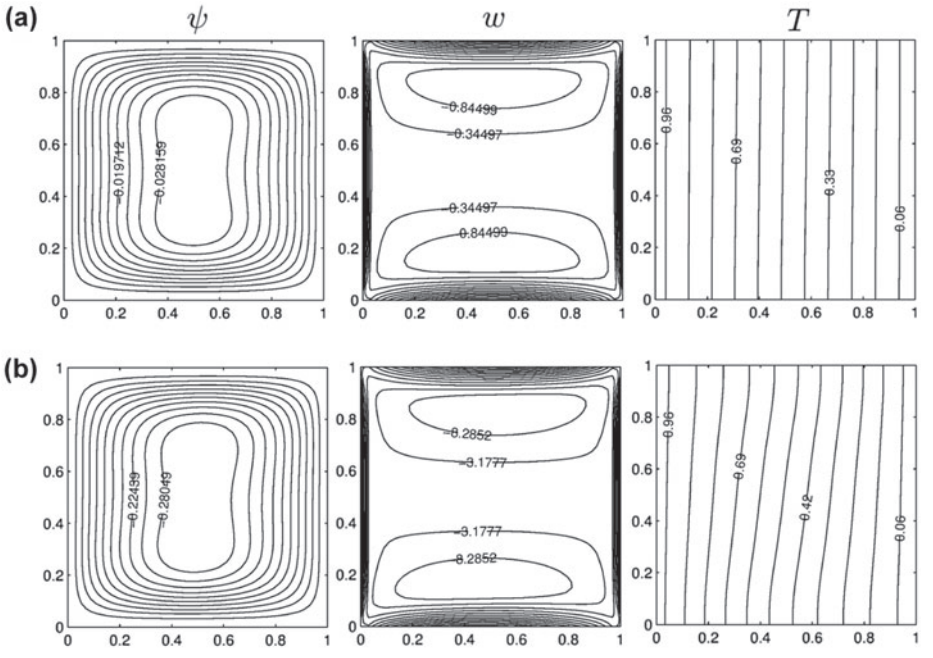

Figure 4. Streamlines, vorticity contours and isotherms by DRBEM for $Ha = 60, \phi = 0.03, \gamma = 0$: (a) $Ra = 10^3$, (b) $Ra = 10^4$.

$0, 0.03, 0.08, 0.15, 0.2$) is displayed in Figure 6(a) for $Ha = 10$ and Figure 6(b) for $Ha = 60$ when $Ra = 10^5$, $\gamma = 0$. The results are obtained using DRBEM. It is observed that the Hartmann number has a crucial effect on the nanofluid flow at various values of the solid volume fraction. As the solid volume fraction increases, the stream function and vorticity values increase in magnitude for small values of Hartmann number as $Ha = 10$. However, the stream function values decrease in magnitude with an increase in ϕ for a higher value of Hartmann number, namely $Ha = 60$, which indicates a reduction in the fluid flow rate along the vertical centreline of the cavity, and a decrease in the strength of the convective circulations. On the other hand, there is no significant effect of ϕ on the vorticity variation when $Ha = 60$. Increasing ϕ has also no effect on the values of temperature for small $Ha = 10$, whereas the temperature increases in the lower part of the cavity ($0 < y < 0.5$) and it decreases in the upper part ($0.5 < y < 1$) when $Ha = 60$. The calculations are also carried out for the values of Hartmann number ($10 < Ha < 60$); and it is observed that $Ha \approx 25$ is a critical value at $Ra = 10^5$. That is, for higher values of Hartmann number ($Ha \geq 25$), an increase in ϕ results in a reduction in magnitude of stream function, while it increases for $Ha < 25$.

It is well-known that one has to use finer mesh when Ra increases. DRBEM matrices are full matrices and do not show a special form, although their sizes are small due to the boundary-only discretization. Thus, they present difficulties for large Rayleigh numbers because of the resulting rather large-sized systems.

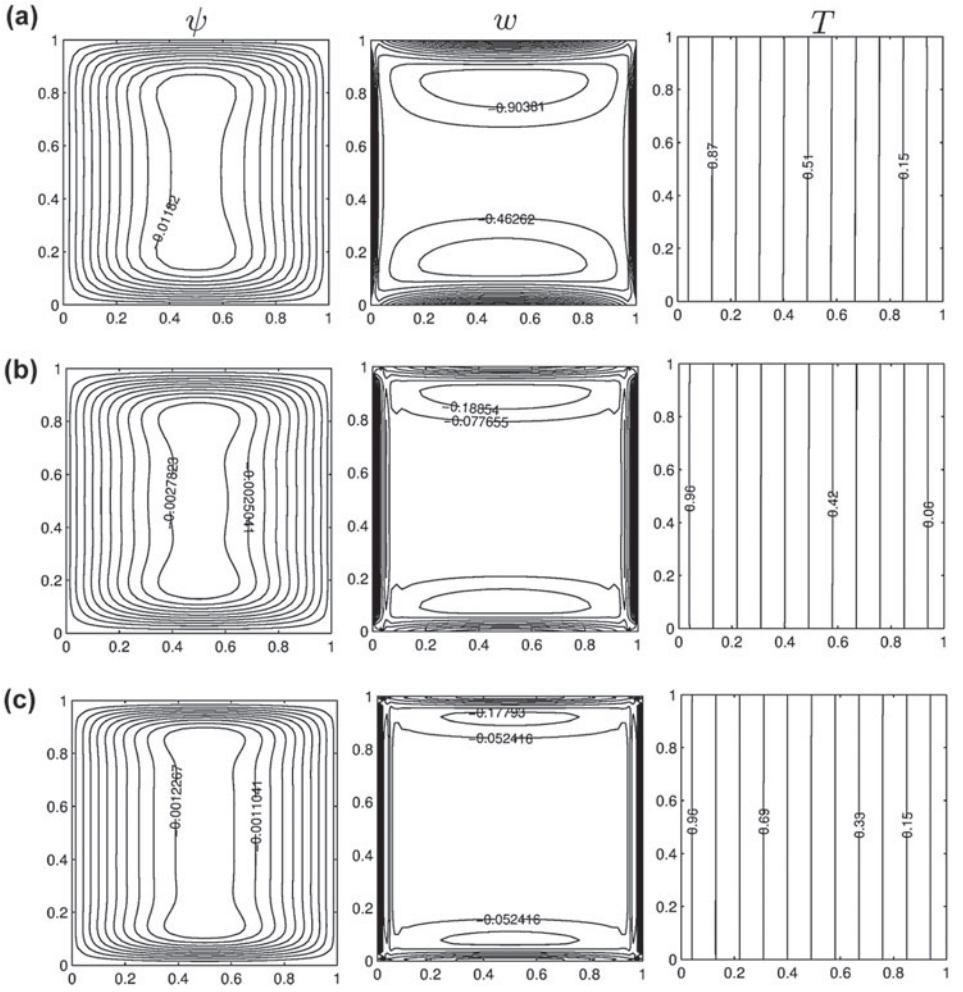

Figure 5. Streamlines, vorticity contours and isotherms by DRBEM for $Ra = 10^3$, $\phi = 0.03$, $\gamma = 0$: (a) $Ha = 100$, (b) $Ha = 200$, (c) $Ha = 300$.

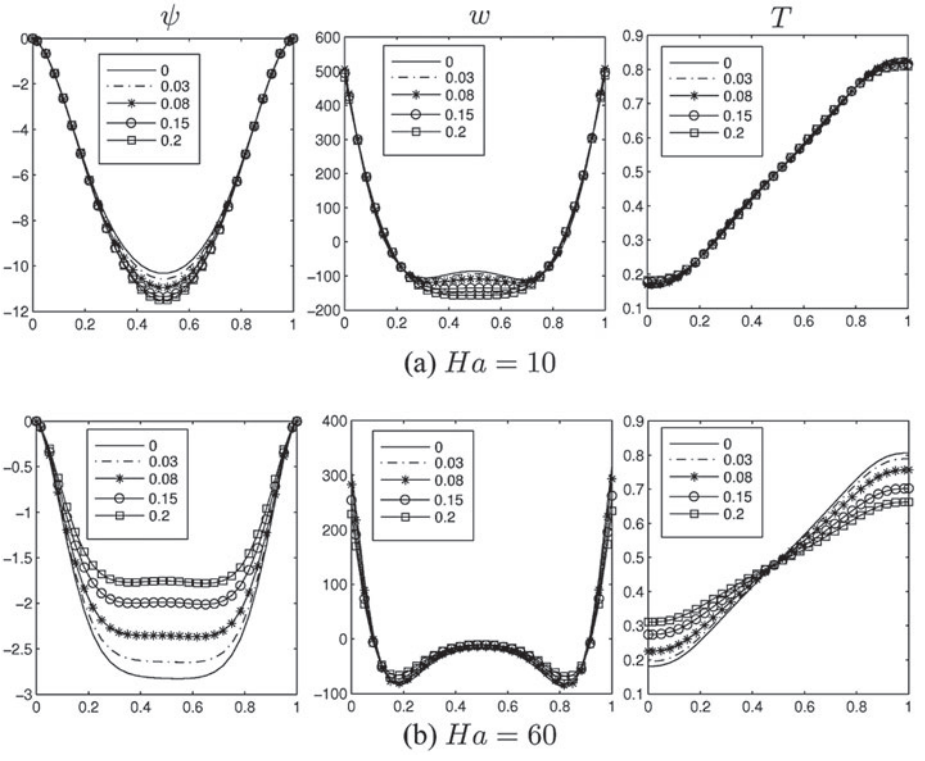

Figure 6. The variation of stream function (left), vorticity (middle) and temperature (right) along the vertical centreline $x = 0.5$, $0 \leq y \leq 1$ at different solid volume fractions ($\phi = 0, 0.03, 0.08, 0.15, 0.2$) for (a) $Ha = 10$, (b) $Ha = 60$ when $Ra = 10^5$, $\gamma = 0$.

However, FEM matrices are sparse while their sizes are large. Thus, for Rayleigh numbers ($Ra > 10^5$), the computations are carried out using FEM. In Figure 7, the FEM solutions are illustrated for $Ha = 100$, $\phi = 0.03$, $\gamma = 0$, and (a) $Ra = 10^4$, (b) $Ra = 10^6$. When Rayleigh number is increased, the strength of the buoyancy-driven circulation increases and undergoes an inversion which is an indication of convection dominance in the flow. The convective transfer increases. As a consequence, the isotherms tend to have changed profiles from vertical to horizontal. These results are in good agreement with the ones obtained in Ghasemi et al. (2011).

The effect of increasing Hartmann number is investigated also for a high Rayleigh number, $Ra = 10^7$ using FEM, and the results are illustrated in Figure 8. It is observed that the horizontal profiles of the streamlines and isotherms are slightly distorted into a diagonal form. The magnitudes of both the streamlines and the vorticity contours are decreased showing the flattening tendency of MHD flow. The convection domination effect on the flow due to the high Rayleigh number is slightly overwhelmed by an increase in the values of Hartmann number from 150 to 300. It is expected to be more pronounced for higher values of Ha.

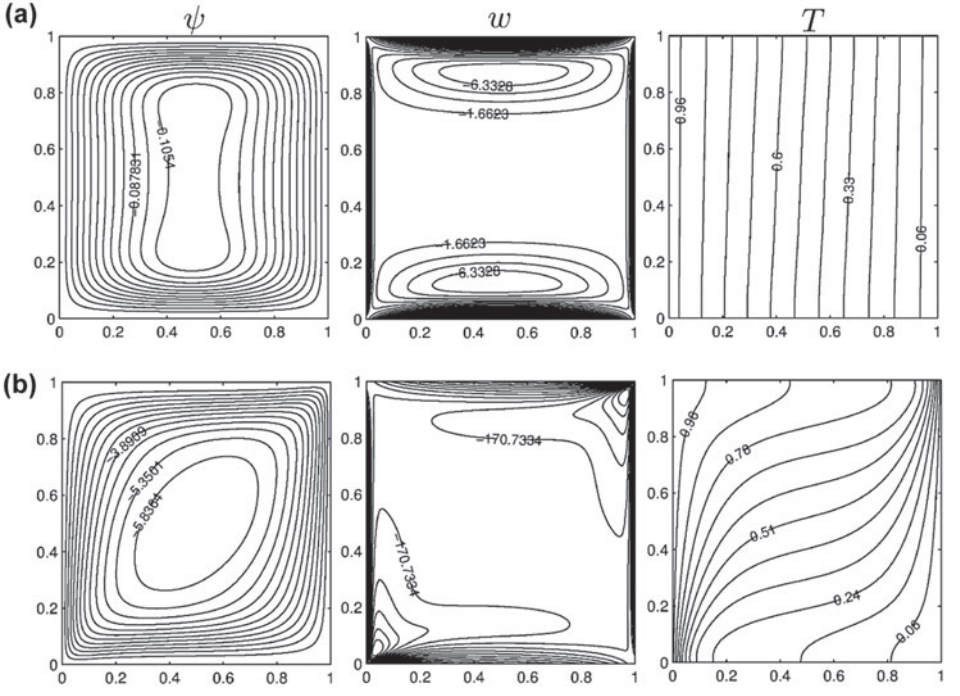

Figure 7. Streamlines, vorticity contours and isotherms by FEM for $Ha = 100$, $\phi = 0.03$, $\gamma = 0$: (a) $Ra = 10^4$, (b) $Ra = 10^6$.

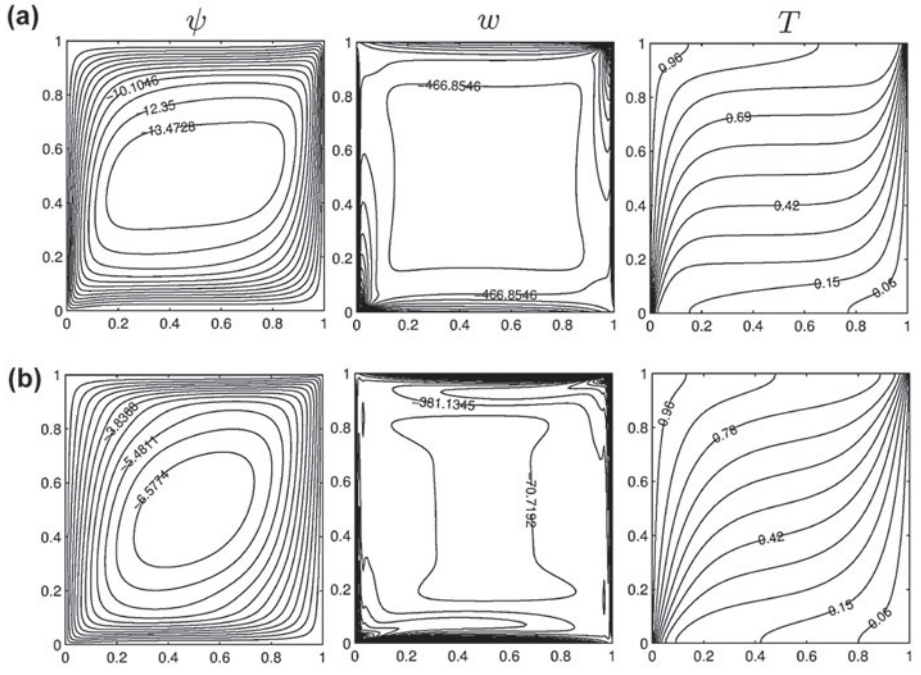

Figure 8. Streamlines, vorticity contours and isotherms by FEM for $Ra = 10^7$, $\phi = 0.03$, $\gamma = 0$: (a) $Ha = 150$, (b) $Ha = 300$.

The streamlines, equivorticity lines and the isotherms are drawn in Figures 9–11 for the Rayleigh numbers $Ra = 10^3$, 10^4, 10^5, respectively, to see the effect of the inclination angle on the flow and the heat transfer, for both the numerical techniques (a) DRBEM and (b) FEM. The results are obtained at $Ha = 60$, $\phi = 0.03$ when $\gamma = \frac{\pi}{4}$ and $\frac{\pi}{3}$. The core vortex of the streamlines, which is almost vertical in the centre of the cavity when $\gamma = 0$ (see Figure 3(a)), extends in the direction of the applied magnetic field. However, the isotherms show the same behaviour, irrespective of the inclination angle γ. Moreover, these figures indicate that the DRBEM and FEM solutions are also in very good agreement for all Ra, and the angles $\gamma = \frac{\pi}{4}$ and $\gamma = \frac{\pi}{3}$ as for the previous cases (when $\gamma = 0$).

The effect of the magnetic field direction is displayed in Figure 12 for inclination angles $\gamma = \frac{\pi}{4}, \frac{\pi}{3}$ and $\frac{\pi}{2}$ when $\phi = 0.03$, $Ra = 10^7$, $Ha = 300$ using FEM. When Figure 12 is compared with Figure 8(b) drawn at the same values of Ra, Ha and ϕ with horizontally applied magnetic field ($\gamma = 0$), it is evident that the direction of the external magnetic field has a considerable effect on the flow. The streamlines and vorticity contours extend along the magnetic field direction. The central vortex in streamlines elongates in the magnetic field direction, and it splits into two symmetric vortices in the same direction for the values $\gamma = \frac{\pi}{3}$ and $\gamma = \frac{\pi}{2}$. The direction of the magnetic field has a similar effect on the

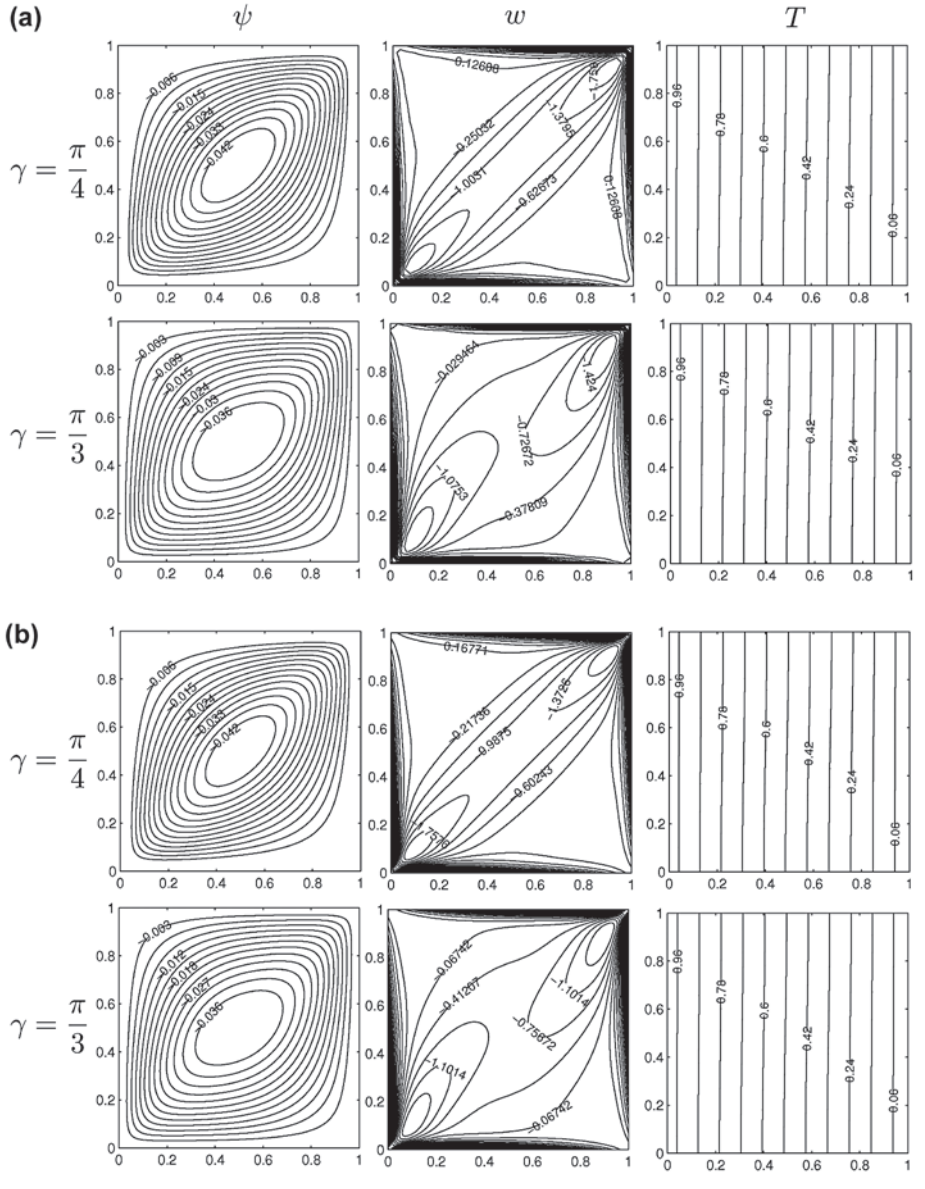

Figure 9. Streamlines, vorticity contours and isotherms for $Ha = 60$, $Ra = 10^3$, $\phi = 0.03$ at $\gamma = \frac{\pi}{4}, \frac{\pi}{3}$: (a) DRBEM, (b) FEM.

vorticity, and the formation of boundary layers is more pronounced along the magnetic field direction. Due to the strong convection for high value of Rayleigh number ($Ra = 10^7$), the magnetic field direction has an insignificant influence on the temperature profile when $\gamma = \frac{\pi}{4}$ and $\gamma = \frac{\pi}{3}$ (see Figures 8(b) and 12(a)–(b)). Magnetic field applied in the vertical direction ($\gamma = \frac{\pi}{2}$) is slightly more effective in forming boundary layers in streamlines and vorticity contours

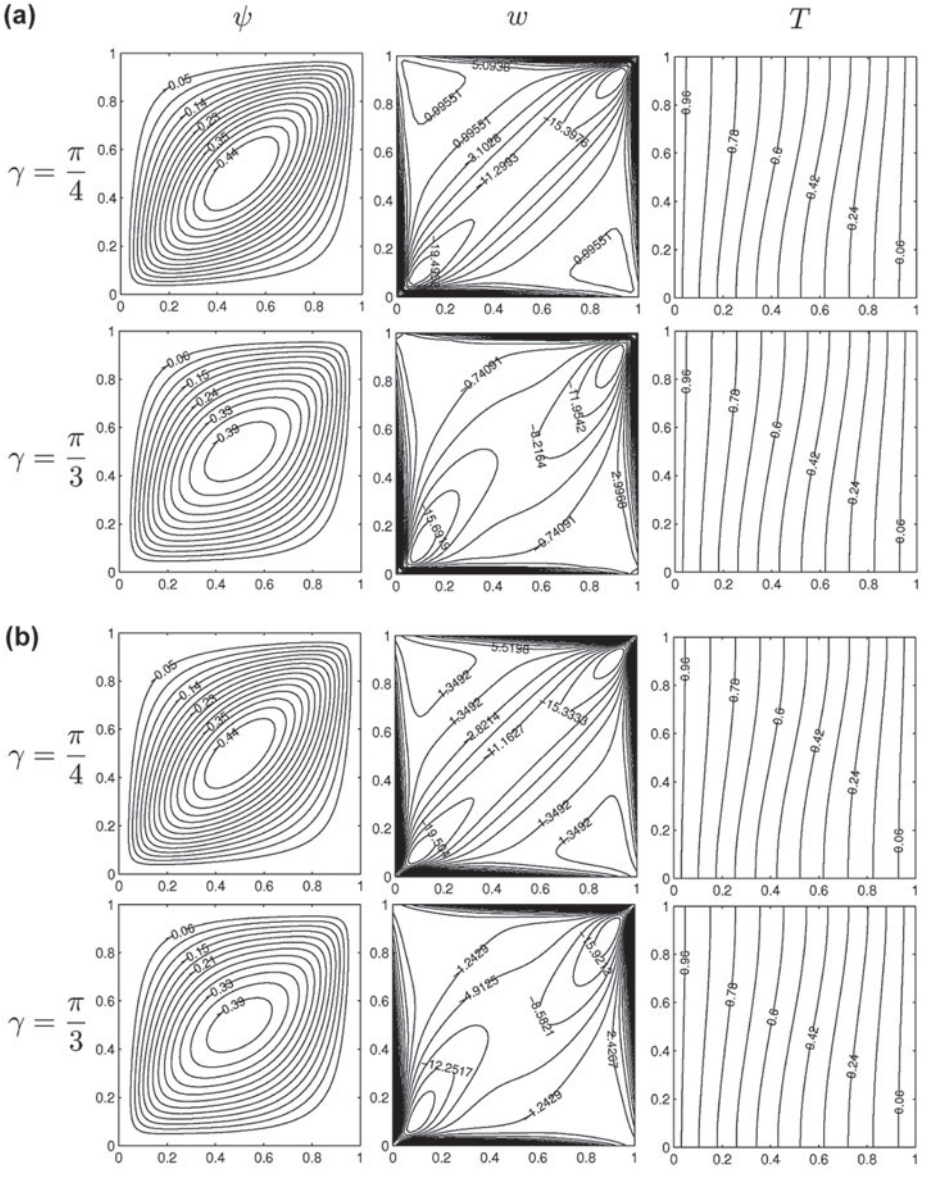

Figure 10. Streamlines, vorticity contours and isotherms for $Ha = 60$, $Ra = 10^4$, $\phi = 0.03$ at $\gamma = \frac{\pi}{4}, \frac{\pi}{3}$: (a) DRBEM, (b) FEM.

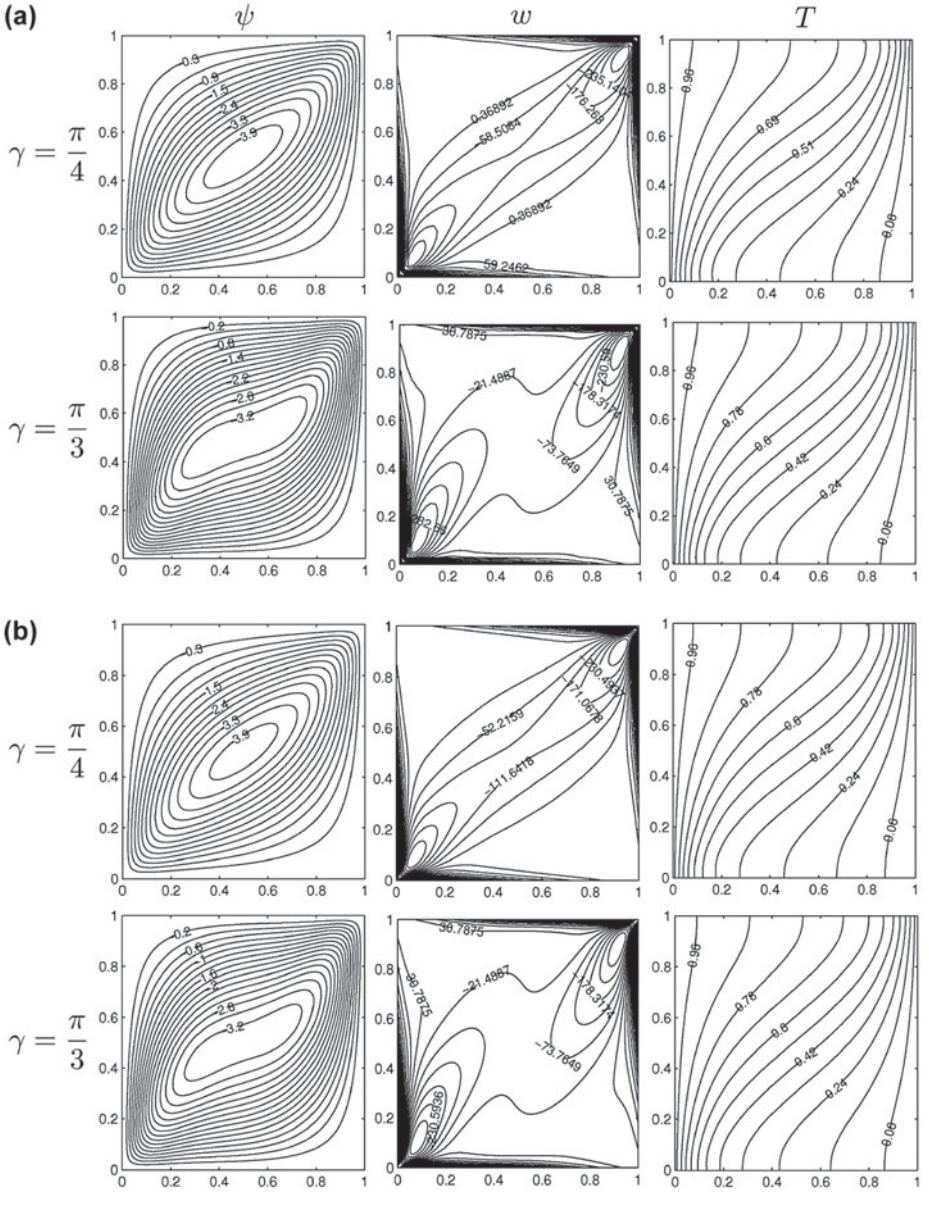

Figure 11. Streamlines, vorticity contours and isotherms for $Ha = 60$, $Ra = 10^5$, $\phi = 0.03$ at $\gamma = \frac{\pi}{4}, \frac{\pi}{3}$: (a) DRBEM, (b) FEM.

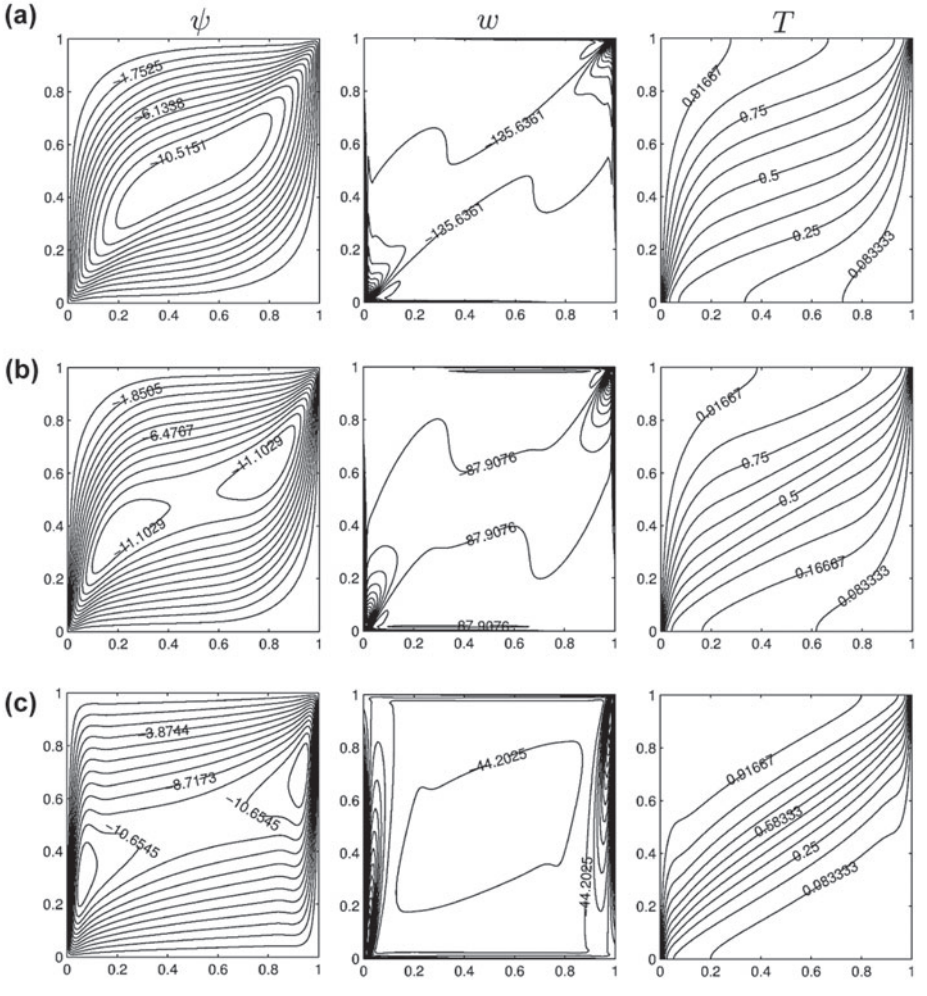

Figure 12. Streamlines, vorticity contours and isotherms by FEM for $Ra = 10^7$, $Ha = 300$, $\phi = 0.03$: (a) $\gamma = \frac{\pi}{4}$, (b) $\gamma = \frac{\pi}{3}$, (c) $\gamma = \frac{\pi}{2}$.

along the vertical walls. This effect is also observed on heat transfer as isotherms are shifted through the diagonal of the cavity.

5. Conclusion

The natural convection flow in an enclosure filled with a water/alumina nanofluid is solved under the effect of an inclined magnetic field using two numerical techniques, namely: FEM and DRBEM, with different meshing types. Both FEM and DRBEM are suitable approaches for simulating MHD natural convection heat transfer of nanofluids in enclosures. For moderate values of *Ra* and *Ha*, they give the same behaviour of the flow and temperature. The FEM is more powerful to solve the problem for high values of *Ra* and *Ha*; however, the DRBEM computational cost is considerably less. The effects of the physical problem parameters on the flow behaviour and the temperature distribution are investigated. It is observed that an increase in Hartmann number results in a decrease in the magnitude of stream function and vorticity, whereas they increase as Rayleigh number increases. Thus, the magnetic field has a negative effect on buoyancy force and decreases the flow motion. Furthermore, the flow becomes convection dominated for high values of *Ra* which leads to a horizontal profile for isotherms. On the other hand, an increase in *Ha* has an opposite effect on the profiles of isotherms, that is the isotherms become vertical following the reduction in the effect of convection. The effect of solid volume fraction on the fluid flow depends on the values of *Ra* and *Ha*, e.g. at $Ra = 10^5$, the magnitude of the stream function increases for $Ha < 25$, but decreases for $Ha \geq 25$ with an increase in the solid volume fraction. The results obtained using DRBEM and FEM are in good agreement with each other for all inclination angles tested, and also with the results given in the literature (Ghasemi et al., 2011) when $\gamma = 0$. The flow pattern is considerably affected by the variation in the magnetic field direction. Moreover, as the inclination of the external magnetic field is increasing from 0 to $\pi/2$, the heat transfer is finally confined between the left lower and right upper corners of the cavity.

Disclosure statement

No potential conflict of interest was reported by the authors.

References

Brebbia, C. A., Partridge, P. W., & Wrobel, L. C. (1992). *The dual reciprocity boundary element method*. Southampton: Computational Mechanics Publications.

Elshehabey, H. M., Hady, F. M., Ahmed, S. E., & Mohamed, R. A. (2014). Numerical investigation for natural convection of a nanofluid in an inclined L-shaped cavity in the presence of an inclined magnetic field. *International Communications in Heat and Mass Transfer, 57*, 228–238.

Ghasemi, B. (2013). Magnetohydrodynamic natural convection of nanofluids in U-shaped enclosures. *Numerical Heat Transfer, Part A: Applications, 63*, 473–487.

Ghasemi, B., Aminossadati, S. M., & Raisi, A. (2011). Magnetic field effect on natural convection in a nanofluid-filled square enclosure. *International Journal of Thermal Sciences, 50*, 1748–1756.

Gümgüm, S., & Tezer-Sezgin, M. (2010). DRBEM solution of natural convection flow of nanofluids with a heat source. *Engineering Analysis with Boundary Elements, 34*, 727–737.

Hasanuzzaman, M., Öztop, H. F., Rahman, M., Rahim, N., Saidur, R., & Varol, Y. (2012). Magnetohydrodynamic natural convection in trapezoidal cavities. *International Communications in Heat and Mass Transfer, 39*, 1384–1394.

Hamida, M. B., & Charrada, K. (2015). Natural convection heat transfer in an enclosure filled with an ethylene glycol-copper nanofluid under magnetic fields. *Numerical Heat Transfer, Part A, 67*, 902–920.

Hossain, M. S., & Alim, M. A. (2014). MHD free convection within trapezoidal cavity with non-uniformly heated bottom wall. *International Journal of Heat and Mass Transfer, 69*, 327–336.

Kefayati, G. (2013). Effect of a magnetic field on natural convection in an open cavity subjugated to water/alumina nanofluid using lattice boltzmann method. *International Communications in Heat and Mass Transfer, 40*, 67–77.

Mahmoudi, A. H., Pop, I., & Shahi, M. (2012). Effect of magnetic field on natural convection in a triangular enclosure filled with nanofluid. *International Journal of Thermal Sciences, 59*, 126–140.

Öztop, H., Al-Salem, K., & Pop, I. (2011). MHD mixed convection in a lid-driven cavity with corner heater. *International Journal of Heat and Mass Transfer, 54*, 3494–3504.

Pirmohammadi, M., & Ghassemi, M. (2009). Effect of magnetic field on convection heat transfer inside a tilted square enclosure. *International Communications in Heat and Mass Transfer, 36*, 776–780.

Reddy, J. N. (2006). *An introduction to the finite element method*. New York: The McGraw-Hill Companies.

Sheikholeslami, M., & Ganji, D. D. (2014). Ferrohydrodynamic and magnetohydrodynamic effects on ferrofluid flow and convective heat transfer. *Energy, 75*, 400–410.

Sheikholeslami, M., Gorji-Bandpy, M., & Ganji, D. (2013). Numerical investigation of MHD effects on Al_2O_3 water nanofluid flow and heat transfer in a semi-annulus enclosure using LBM. *Energy, 60*, 501–510.

Sheikholeslami, M., Gorji-Bandpy, M., Ganji, D. D., & Soleimani, S. (2014). MHD natural convection in a nanofluid filled inclined enclosure with sinusoidal wall using CVFEM. *Neural Computing & Applications, 24*, 873–882.

Türk, O., & Tezer-Sezgin, M. (2013). FEM solution of natural convection flow in square enclosures under magnetic field. *International Journal of Numerical Methods for Heat & Fluid Flow, 23*, 844–866.

Yu, P., Qiu, J., Qin, Q., & Tian, Z. (2013). Numerical investigation of natural convection in a rectangular cavity under different directions of uniform magnetic field. *International Journal of Heat and Mass Transfer, 67*, 1131–1344.